

Amplitude quantization method for autonomous threshold estimation in self-reconfigurable cognitive radio systems

A. J. Onumanyi^{a,*}, A. M. Abu-Mahfouz^{b,a} and G. P. Hancke^{c,a}

^aUniversity of Pretoria, Pretoria, South Africa

^bCouncil for Scientific and Industrial Research, Pretoria, South Africa

^cDepartment of Computer Science, City University of Hong Kong, Hong Kong, China

ARTICLE INFO

Keywords:

Adaptive

Algorithm

Autonomous

Cognitive Radio

Networks

Signal detection.

ABSTRACT

Self-adaptive threshold adjustment algorithms (SATAs) are required to reconfigure their parameters autonomously (i.e. to achieve self-parameter adjustment) at runtime and during online use for effective signal detection in cognitive radio (CR) applications. In this regard, a CR system embedded with the functionality of a SATA is termed a self-reconfigurable CR system. However, SATAs are challenging to develop owing to a lack of methods for self-parameter adjustment. Thus, a plausible approach towards realizing a functional SATA may involve developing effective non-parametric methods, which are often pliable to achieve self-parameter adjustment since they are distribution-free methods. In this article, we introduce such a method termed the non-parametric amplitude quantization method (NPAQM) designed to improve primary user signal detection in CR without requiring its parameters to be manually fine-tuned. The NPAQM works by quantizing the amplitude of an input signal and then evaluating each quantized value based on the principle of discriminant analysis. Then, the algorithm searches for an effective threshold value that maximally separates noise from signal elements in the input signal sample. Further, we propose a new heuristic, which is an algorithm designed based on a new corollary derived from the Otsu's algorithm towards improving the NPAQM's performance under noise-only regimes. We applied our method to the case of the energy detector and compared the NPAQM with other autonomous methods. We show that the NPAQM provides improved performance as against known methods, particularly in terms of maintaining a low probability of false alarm under different test conditions.

1. Introduction

Cognitive radio (CR) refers to an adaptive radio that can detect and use free channels (white spaces) on a non-interference basis for opportunistic communication [1]. CR systems are deployed in many communication networks based on the IEEE 802.22 standard in order to improve user perceived quality of service as well as to improve the spectra utilization and efficiency of existing communication networks. CR systems are also deployed to extend the coverage area of modern networks by ensuring that signals are transmitted in lower frequency bands wherein they can propagate much farther in space [2]. Essentially, most CR systems are

*Corresponding author

 adeiza1@futminna.edu.ng (A.J. Onumanyi)

ORCID(s):

required to sense their surrounding spectra towards deciding accurately whether primary user (PU) signals are present (occupied) or absent (free) in a specified channel. In order to achieve this, most CR systems are deployed using either one or a combination of different detectors, such as the radiometer (popularly called the energy detector (ED)), cyclostationary detector, matched filter, Eigen value detector or the compressed sensing method [1]. However, the ED is widely considered to be the most viable detector since it suffices as the simplest, fastest, cheapest, and least computationally-demanding detector [1–3]. In principle, the ED works by estimating accurate threshold values based on the magnitude of the elements in the input sample, and then such threshold values are used to determine correctly whether PU signals exist or not in the sensed channel [4–6]. However, because noise elements are random and fluctuate unpredictably, consequently, it is required that CR systems should be embedded with effective adaptive threshold adjustment algorithms (ATAs), which are able to accurately compute and adapt the threshold of an ED under vacillating noise levels [7–11].

In this regard, a number of ATAs are well-known in the literature for their effectiveness. However, most of these ATAs are predominantly parametric-based methods that depend on manually fine-tuned parameters before they can be used. These parameters are often computed and fine-tuned by a human operator at runtime and thus such parameters cannot be readjusted (i.e reconfigured) until the next runtime. Even so, in cases where wrong values are assigned to these parameters, the performance of a CR system can be severely undermined. This may lead either to very low probability of detection (P_D) or very high probability of false alarm (P_{FA}) of the CR system. Most importantly, there are some recent CR-based applications, such as in CR-based wireless sensor networks (WSNs) where remotely deployed CR-based sensors are required. These sensors are often unreachable after being deployed, and thus are required to autonomously readjust their parameters based only on the input data sample acquired per time [12]. In this regard, we define such ATAs that are capable of self-reconfiguring their parameters at runtime and during online use without human intervention as self-adaptive threshold adjustment algorithms (SATAs).

It is difficult to design SATAs using commonly available parametric-based ATAs because of a lack of valid methods to achieve self-parameter adjustment in such parametric-based methods. Thus, an approach towards developing SATAs may involve constructing non-parametric-based threshold adjustment approaches, which can be extended easily to become fully self-adaptive methods. Further, non-parametric methods are suitable for use because by being distribution-free in nature, they are typically independent of the unknown

parameters of many probability distribution functions often associated with most parametric-based methods. In this regard, we note that non-parametric methods are methods that do not require that the signal of interest being analysed meets certain assumptions about its underlying probability distribution. Put simply, the parameters are not fixed and neither is the type of probability distribution used in the method to model the input signal. In the strict sense, they are called distribution-free methods because it is not required that any probability distribution be assumed in order to construct the method [13]. On the other hand, parametric methods depend on a set of fixed parameters of a suitable probability distribution used to construct the method. Essentially, in most parametric methods, the input data is often assumed to originate from a certain distribution, which is assumed to be known *a priori* as well as its parameters [13]. Consequently, we approach a new pertinent research question in the present article, which is, how can a self-adaptive and non-parametric (distribution-free) method be developed for useful threshold estimation in CR applications? We note that if such methods are developed, they will be highly useful, particularly for CR-based applications where remotely deployed self-reconfiguring sensors are required, for example in military, marine, geological-based WSN, and other IoT-based applications [14–16]. Further, developing such methods will provide the following benefits: SATAs deployed in CR systems will experience fewer cases of erroneously determined parameter values, which are typically caused by human mistakes during the fine-tuning process. SATAs will be able to accurately and automatically adjust their parameter values towards matching changing spectra conditions, and CR systems will be able to react much quicker to sudden changes in spectra conditions.

Thus, in the present article, we propose a method called the non-parametric amplitude quantization method (NPAQM) for estimating accurate threshold values by self-adjusting its internal parameters. The NPAQM is a SATA since it can autonomously adjust its internal parameters at runtime and during online use. To realize these characteristics, the NPAQM works by evaluating a set of potential threshold values obtained by quantizing the magnitude of the frequency domain input signal. It then measures the *goodness* of each threshold value using the first order difference of the between-class variance function derived from the Otsu's algorithm. This enables the NPAQM to compute a candidate threshold value that maximally separates noise from signal elements in an input signal sample. In addition, a corollary is derived from the principle of discriminant analysis behind the Otsu's algorithm, from which a new heuristic is constructed that maintains a low false alarm rate for the NPAQM under noise-only regimes. We evaluated the NPAQM extensively

under different possible operating conditions and our findings have led to the following contributions:

1. We have developed a new self-adaptive and non-parametric threshold adjustment algorithm called the NPAQM, which does not require gray-scale level computations or histogram generation as obtained in existing methods.
2. We have derived a new and interesting corollary from the Otsu's algorithm to determine the unimodality of an unknown distribution. We then constructed a new heuristic algorithm based on the corollary to improve the NPAQM's performance under noise-only regimes, a condition in which many existing methods typically under-perform. This heuristic algorithm is described in Section 4.3.
3. The NPAQM selects an effective threshold value using the first order difference of the between-class variance function, which differentiates the NPAQM from existing methods. It was extensively tested and compared with existing non-parametric methods under different operating conditions and shown to achieve improved performance.

The rest of the article is structured as follows: the related work is discussed in Section 2. The detection system is presented in Section 3 and full details of the NPAQM is provided in Section 4. Our method of analysis is elucidated in Section 5. The results obtained are presented and discussed in Section 6, while conclusions are drawn in Section 7.

2. Related Work

There are two main threshold estimation approaches deployed in most ED-based CR systems namely, the fixed and adaptive threshold estimation methods. Some recent use-cases of the fixed threshold approach can be found in [4–6]. However, since the fixed approach cannot adapt to fluctuating spectra conditions, consequently, its performance declines under conditions of noise uncertainty, fading, interference, and the general randomness from thermal and ambient noise measurements [7, 9, 11]. As a consequence, recent attention has been drawn to the importance of ATAs since they naturally outperform the fixed threshold approach. In this regard, ATAs can be further grouped into two broad classes namely, the parametric and non-parametric-based methods.

In most cases, many notable ATAs are parametric-based algorithms, which depend on presumed noise distributions for their configuration. The forward consecutive mean excision (FCME) algorithm is an example of a popular ATA that depends on two basic parameters, namely the threshold factor T_{cme} and the

percentage of clean elements Q [17, 18]. In [18], authors configured the FCME algorithm using different noise distributions, such as the exponential distribution to develop theoretical formulas to compute T_{cme} , while assuming different values for Q . In practice, such theoretically assumed distributions may deviate from the actual ground-truth, for example in cases where a small number of elements are sensed. This may lead to poorly estimated parameter values that may undermine the performance of the FCME algorithm.

A similar argument suffices for other ATAs such as the recursive one-sided hypothesis testing (ROHT) technique [19], and the first order statistical technique (FOST) [20], Barne's approach [21], and many other methods as in [22–26]. Essentially, these methods depend on critical parameters that are fine-tuned *a priori* based on some input noise level or some theoretical distribution of the input sample. However, once these values are defined, it is often impossible to adjust their parameter values autonomously during online/realtime use, thus lacking the characteristics required of a SATA. Furthermore, these methods may assume more about a given sample distribution as against non-parametric methods. When these assumptions are correct, parametric ATAs are able to estimate more accurate threshold values than most non-parametric methods. However, since more is often assumed by parametric ATAs, thus, when these assumptions are incorrect, these methods typically fail, which limits their robustness.

Consequently, the present article focuses on non-parametric ATAs, which are typically distribution-free methods [27]. To the best of our knowledge, we have identified two different non-parametric methods deployed in the literature for signal detection in CR applications. The first approach appears in [19], which adopts the Otsu's algorithm in order to estimate accurate threshold values for ED-based CR systems. Therein, authors computed the gray-scale level and histogram of the input sample and applied Otsu's algorithm to compute accurate threshold values. However, in a later publication, authors in [9] noted that Datla's approach in [19] may be limited in two ways: first, it was found that using Otsu's algorithm introduces significant processing delay since there is need to compute gray-scale levels. Second, Datla's approach becomes limited under noise-only conditions since it has no mechanism to determine this case. Consequently, such limitations were avoided in [9] by circumventing the need to compute gray-scale levels albeit the need to compute histograms, which further limits the algorithm's performance. Thus, different from these approaches, we seek to alleviate the aforementioned limitations by circumventing the need for both gray-scale and histogram computations. In this regard, we introduce a new method in Section 4 as well as a heuristic algorithm that maintains a low false alarm rate for our method under noise-only regimes. Our proposed methods and the

new test for the unimodality of an unknown distribution are contributions that distinguish the present article from existing works. There are many future CR-based applications that may benefit from our proposed technique, possibly in future Internet of Things (IoT)-based applications in 5G [28] as well as in cluster-based CR applications in industrial IoT [29].

3. The Detection System

Figure 1 presents the front-end model of an energy detector (ED) deployable for signal detection in CR applications. The model comprises an adaptive threshold adjustment block in which our proposed algorithm is deployed. Essentially, the input signal, which is often corrupted by channel effects such as fading and ambient/device noise is received via the input antenna. The received signal $y(t)$ is modelled as

$$H_0 : y(t) = w(t); \text{ for } t = 1, 2, \dots, N \quad (1)$$

$$H_1 : y(t) = h(t) * s(t) + w(t); \text{ for } t = 1, 2, \dots, N \quad (2)$$

where t is the time index, N is the total number of time-domain elements, $h(t)$ is the channel impulse response function, $s(t)$ is the transmitted signal, $w(t)$ is the ambient/system noise modelled as additive white Gaussian noise (AWGN), and the symbol '*' denotes the convolution operator. In this case, N is obtained as $N = \lceil T_s \times f_s \rceil$, where $\lceil \cdot \rceil$ denotes the ceiling function, T_s is the total sensing period, and f_s is the sampling frequency. The H_0 hypothesis describes the case where the received signal comprises elements of a noise-only sample, whereas H_1 corresponds to the case where the received signal comprises elements of a signal-plus-noise sample. We consider the channel response function $h(t)$ as described by Rayleigh fading distribution. Rayleigh distribution was considered since it is most applicable in non-line of sight communication networks deployed in heavily built-up urban environments [30]. In our simulation, we used Jake's model based on summing sinusoids to simulate Rayleigh fading channels following the approach in [31]. Furthermore, we considered the case for frequency-flat fading channels in our simulation since our concern has to do with television white spaces (TVWS), which are typically less than 6MHz in bandwidth. In this case, such a bandwidth size and less would typically experience to a greater extent frequency-flat fading channels as against frequency-selective fading channels, which arise more often in broadband channels [32].

Generally, since our method operates upon frequency domain-based elements, thus, the ED computes in

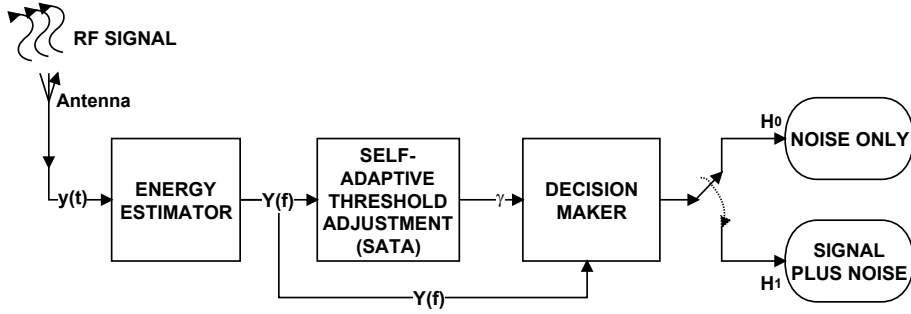


Figure 1: A simple front-end model of an ED-based CR system

the energy estimator block the power spectral density (PSD) of $y(t)$ as $Y(f)$, where f denotes the frequency index of each channel. For this purpose, we used the fast Fourier transformation (FFT) algorithm to compute $Y(f)$ based on the approach in [33]. Hence, in the frequency domain, the corresponding hypotheses H_0 and H_1 translate to:

$$H_0 : Y(f) = W(f), \text{ for } f = 1, 2, \dots, F \quad (3)$$

$$H_1 : Y(f) = H(f) \cdot S(f) + W(f), \text{ for } f = 1, 2, \dots, F \quad (4)$$

where F is the total number of frequency channels in the measured/sensed bandwidth and other variables therein are the corresponding frequency domain transformed variables of (1) and (2), respectively. Here, F is concisely determined as

$$F = 2^{\lceil (\log_2(T_s \times f_s) - 1) \rceil} \quad (5)$$

A quick derivation of (5) is presented in Appendix A. Then, following Figure 1, the sample $Y(f)$ for $f = 1, 2, 3, \dots, F$ is fed to the self-adaptive threshold adjustment block where processing takes place in order to compute a suitable threshold value γ . Then, each element in $Y(f)$ is compared to γ in the decision maker block towards determining the state of each channel f . It is worth noting that an element in this case refers to a single frequency channel f , whereas a set of elements is considered to be a single sample, which corresponds to a single sweep of a number of contiguous frequency channels (i.e the entire sensed bandwidth). If a channel turns out to be free (i.e. $Y(f) < \gamma$), then we declare H_0 , which implies that the channel contains noise-only elements, whereas, if the channel is occupied (i.e. $Y(f) \geq \gamma$), then we declare

H_1 , which implies that the channel contains signal-plus-noise elements.

In subsequent sections of this article, we shall refer to $Y(f)$ simply as Y_f , where f maintains its meaning as the frequency channel index and F remains the total number of frequency channels. In essence, we aim in the present article to compute effective γ values using our newly proposed method in order to accurately decide which of the cases (i.e. H_0 or H_1) may suffice under different channel conditions.

4. The Proposed Method

In this section, we describe the non-parametric amplitude quantization method (NPAQM) and derive an interesting corollary from the theoretical basis of the Otsu's algorithm. We then present a new heuristic algorithm based on the new corollary in order to improve the NPAQM's performance under noise-only regimes. This section closes with an analysis of the time complexity of the NPAQM.

4.1. The Non-parametric Amplitude Quantization Method

We aim to develop an effective SATA deployable in an ED for signal detection in CR applications. Our idea stems from the non-parametric approach associated with the Otsu's algorithm. In order to construct our method, we consider the PSD sample $Y_f = \{y_1, y_2, \dots, y_F\}$ as the input to our algorithm. The PSD sample is typically obtained via the sensing front-end presented in Figure 1. The total number of elements F is obtained using (5). Since the desired threshold value lies within the magnitude range of Y_f , an intuitive approach to determine this value is to first quantize Y_f into discrete values and then evaluate each discrete value to determine their respective levels of effectiveness. The idea of quantization is introduced to limit the search space for the candidate threshold value. In most cases, the amplitude range of the input signal may be quite large to search every single value in order to determine the best choice of the threshold value. Consequently, it is more efficient to quantize the magnitude range and then to test each quantized value instead of all possible values towards determining the best threshold value. Thus, in order to effectively quantize Y_f , we adopt Doane's formula in [34] to automatically determine the desired quantization level M suited for Y_f . Doane's formula was considered because of its simplicity as well as for its effectiveness over non-normal data, which is often encountered in many communication networks [13]. Thus, the NPAQM

computes the quantization level M as [34]:

$$M = \left\lceil 1 + \log_2 F + \log_2 \left(1 + \frac{|g|}{\sigma_g} \right) \right\rceil, \quad (6)$$

where $|\cdot|$ refers to the modulus function, $\lceil \cdot \rceil$ is the ceiling function, and g is the estimated 3rd-moment (skewness) of the distribution obtained as

$$g = \frac{\frac{1}{F} \sum_{i=1}^F (Y_i - \bar{Y}_f)^3}{\left(\frac{1}{F} \sum_{i=1}^F (Y_i - \bar{Y}_f)^2 \right)^{\frac{3}{2}}}, \quad (7)$$

where \bar{Y}_f denotes the mean of the input sample set Y_f and

$$\sigma_g = \sqrt{\frac{6(F-2)}{(F+1)(F+3)}}. \quad (8)$$

Next, in order to determine the quantization step size q for Y_f , the NPAQM reorders the elements in Y_f as follows: $Y_{(f)} = \{y_{(1)}, y_{(2)}, \dots, y_{(F)}\}$, where $Y_{(f)}$ is sorted in an ascending order such that $y_{(1)} < y_{(2)} < \dots < y_{(F)}$. This reordering process enables the NPAQM to obtain a set of potential threshold values, which will be examined to determine the most effective value for signal detection. To achieve this, we compute q based on M as

$$q = \left\lceil \frac{y_{(F)} - y_{(1)}}{M} \right\rceil, \quad (9)$$

By using q , the NPAQM then obtains the reordered quantized values of $Y_{(f)}$ as $Y_{(m)}$, where $Y_{(m)} = \{y_{(1)}, y_{(1)} + q, y_{(1)} + 2q, \dots, y_{(1)} + (M-1)q\}$. This process is a step further towards constructing a set of potential threshold values required for signal detection. However, for sake of clarity, we rewrite $Y_{(m)}$ simply as $Y_{(m)} = \{y_{(1)}, y_{(2)}, \dots, y_{(M)}\}$, where $Y_{(2)} = y_{(1)} + q, Y_{(3)} = y_{(1)} + 2q, \dots, Y_{(M)} = y_{(1)} + (M-1)q$, which are arranged in the following order $y_{(1)} < y_{(2)} < \dots < y_{(M)}$. Each value in $Y_{(m)}$ is considered to be a potential

threshold value and $Y_{(m)}$ is rewritten for notational convenience as γ_i expressed as

$$\gamma_i = \{\gamma_1, \gamma_2, \dots, \gamma_M\}, \quad (10)$$

where $\gamma_1 = y_{(1)}, \gamma_2 = y_{(2)}, \dots, \gamma_M = y_{(M)}$. At this point, we note that γ_i is a collection of potential threshold values. Thus, when applied to Y_f , each value in γ_i would bifurcate Y_f into two subsets, namely the noise-only subset $\omega(\gamma_i)$, and the signal-plus-noise subset $S(\gamma_i)$, where elements with values smaller than γ_i are considered to be noise-only elements, whereas elements with values larger than γ_i are considered to be signal-plus-noise elements. We then obtain the values of $\omega(\gamma_i)$ and $S(\gamma_i)$ as

$$\omega(\gamma_i) = \{Y_{(f)} < \gamma_i\} = \{y_{(1)}, y_{(2)}, \dots, y_{(k)}\}, \quad (11)$$

$$S(\gamma_i) = \{Y_{(f)} \geq \gamma_i\} = \{y_{(k+1)}, y_{(k+2)}, \dots, y_{(F)}\}, \quad (12)$$

for $\gamma_i = \gamma_1, \gamma_2, \dots, \gamma_M$, where k refers to the number of elements in $\omega(\gamma_i)$, that is, the number of elements with values smaller than γ_i . Then, based on the principles of discriminant analysis elucidated in [35], we proceed to compute the between-class variance of the subsets $\omega(\gamma_i)$ and $S(\gamma_i)$ for each threshold element in γ_i as [35]:

$$\sigma^2(\gamma_i) = P_s(\gamma_i) \cdot P_\omega(\gamma_i) \left[\overline{S}(\gamma_i) - \overline{\omega}(\gamma_i) \right]^2, \text{ for } \gamma_i = \gamma_1, \gamma_2, \dots, \gamma_M \quad (13)$$

where P_s is the probability of signal elements in $S(\gamma_i)$, P_ω is the probability of noise elements in $\omega(\gamma_i)$, $\overline{S}(\gamma_i)$ is the mean of the signal subset $S(\gamma_i)$, and $\overline{\omega}(\gamma_i)$ is the mean of the noise elements in $\omega(\gamma_i)$. The simple probabilities P_s and P_ω in (13) are computed as

$$P_\omega(\gamma_i) = \frac{k}{F}, \quad (14)$$

$$P_s(\gamma_i) = 1 - \frac{k}{F}. \quad (15)$$

In the ideal sense, the between-class variance function of (13) is a parabola (specifically, a quadratic function), which should have a vertex point (a point of inflexion) that corresponds to the maximum value of the function. However, in real-world practice, such a single point of inflexion may not always exist for every input sample, as there may be several elements with the same between-class variance value (i.e. multiple

modes). Consequently, the maxima of (13) may for this reason be uniformly distributed across a range of elements, which makes it difficult to determine the most effective boundary (or inflexion point) between the noise and signal elements in an input sample. Therefore, a better approach is to obtain the first derivative of the between-class variance function, which better reflects the initial point of change between the magnitude of the noise and the signal elements in an input sample. In consequence, we apply the first order difference function of (13) in the NPAQM as follows:

$$\lambda_m(\gamma_i) = \left| \sigma_{m+1}^2(\gamma_i) - \sigma_m^2(\gamma_i) \right|, \text{ for } m = 1, 2, \dots, M - 1. \quad (16)$$

and we obtain the most effective threshold γ^{eff} as

$$\lambda(\gamma^{eff}) = \min_{\text{for } \gamma_i = \gamma_1, \gamma_2, \dots, \gamma_M} \lambda(\gamma_i) \quad (17)$$

Thus, the most effective threshold value γ^{eff} is found to be the threshold value that minimizes (17). Essentially, following the constructs described in (6) - (17), we easily summarize the NPAQM as presented in Algorithm 1. Here, Algorithm 1 highlights the fact that the NPAQM does not require gray-scale compu-

Algorithm 1: Non-parametric amplitude quantization method

Input: PSD sample: $Y_f = \{y_1, y_2, \dots, y_F\}$

Output: Effective threshold value, γ^{eff}

- 1 Reorder input PSD in an ascending order as $Y_{(f)} = \{y_{(1)}, y_{(2)}, \dots, y_{(F)}\}$
 - 2 Compute the optimal quantization level M using (6)
 - 3 Compute the quantization step size q using (9)
 - 4 Obtain the ordered quantized values as $Y_{(m)} = \{y_{(1)}, y_{(1)} + q, y_{(1)} + 2q, \dots, y_{(1)} + (M - 1)q\}$
 - 5 Obtain the candidate threshold values γ_i using (10) based on the quantized values $Y_{(m)}$
 - 6 **for** $\gamma_i = \gamma_1, \gamma_2, \dots, \gamma_M$ **do**
 - 7 Compute $\omega(\gamma_i)$ using (11)
 - 8 Compute $S(\gamma_i)$ using (12)
 - 9 Compute $P_\omega(\gamma_i)$ using (14)
 - 10 Compute $P_S(\gamma_i)$ using (15)
 - 11 Compute $\sigma^2(\gamma_i)$ using (13)
 - 12 Compute $\lambda(\gamma_i)$ using (16)
 - 13 **end**
 - 14 Obtain the desired threshold γ^{eff} using (17)
 - 15 Return γ^{eff}
-

tations or the generation of histograms as obtained in other methods (see [9, 19]). By reordering the input

sample, the NPAQM circumvents the need for computing a histogram function as in [9, 19] since it only needs to count the number of elements in just two subsets $\omega(\gamma_i)$ and $S(\gamma_i)$ at each quantized value γ_i (see steps 7 and 8 of Algorithm 1). Further, the NPAQM is indeed a non-parametric approach since it is obviously independent of any presumed noise distribution. In the following subsections, we shall consider the case for automatically controlling the false alarm rate of the NPAQM under noise-only regimes.

4.2. A New Corollary to determine the unimodality of an Unknown Distribution

In the study of CR systems, it is important to develop new and effective methods to autonomously determine when a sample contains only noise elements, which is a case for the test of the unimodality of an unknown distribution. In this regard, we propose a new corollary to determine the unimodality of an input sample arising from an unknown distribution. This corollary would determine whether a measured sample contains only noise elements or not since noise-only elements are typically described by unimodal distributions [13].

As a background to the new corollary, let us consider the sketches in Figure 2, which depict four different cases. The first case in Figure 2a depicts a clear bimodal distribution with two classes c_0 and c_1 , which relates to the class of noise c_0 and signal c_1 elements, respectively. In the case of the bimodal distribution, we know from the theoretical constructs in [35] that the between-class variance $\sigma_b^2(\gamma)$ of a measured sample will always exist, i.e. $\sigma_b^2(\gamma) > 0$, where γ denotes the threshold. However, we consider three other cases in the present article that describe the case for unimodality, which is a more difficult case to determine automatically in practice. These are shown in Figs. 2b - d, respectively. For example, Figure 2b may represent a very low signal-to-noise ratio (SNR) regime obtained in many signal processing applications. Here, the signal elements are totally buried in noise. In Figure 2c, we sketch the distribution of a noise-only sample, while in Figure 2d, the case of a signal-only sample is depicted. In all three cases (Figs. 2b - d), the unimodality of the different distributions is clearly depicted, for which we shall now provide a new corollary to automatically determine this case.

First, we consider a few theoretical constructs associated with the Otsu's algorithm, which are based on the principles of discriminant analysis [35]. In this regard, a typical histogram $p(i)$ obtained from a measured sample $\{Y_f\}_{f=1}^F$, where F is the total number of elements, will normally be generated and quantized into L bins, such as $i = 1, 2, \dots, L$. Based on these L bins, a threshold value γ is sought that bifurcates these bins i

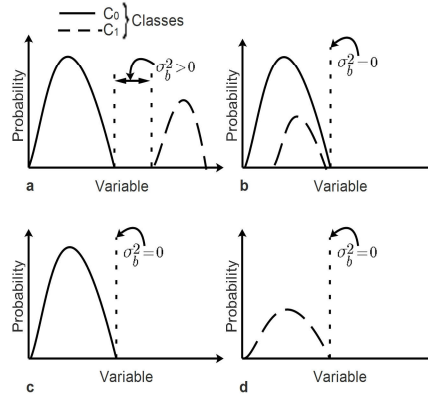


Figure 2: Sketches of Different Density Distributions: (a) Bimodal Distribution, (b) Unimodal Distribution with a mixture of two classes, (c) Unimodal Distribution with a single class, for example, Noise-Only Sample Sets, (d) Unimodal Distribution with a single class, for example, Signal-Only Sample Sets

into two classes c_0 and c_1 , where c_0 consists of $i = 1, 2, \dots, \gamma$ bins, and c_1 consists of $i = \gamma + 1, \gamma + 2, \dots, L$ bins. Otsu has shown in [35] that the optimal γ can be exhaustively searched for by maximizing the inter-class variance of the L bins of the histogram. Furthermore, in [35], the inter-class variance (or between-class variance) function to be maximized is given as:

$$\sigma_b^2(\gamma) = \omega_0 \omega_1 [\mu_0 - \mu_1]^2, \quad (18)$$

which is expressed in terms of class probabilities ω_0 and ω_1 computed as follows:

$$\omega_0 = \sum_{i=1}^{\gamma} p(i) = \omega(\gamma), \quad (19)$$

$$\omega_1 = \sum_{i=\gamma+1}^L p(i) = 1 - \omega(\gamma). \quad (20)$$

and class means μ_0 and μ_1 obtained as

$$\mu_0 = \frac{\sum_{i=1}^{\gamma} i p(i)}{\omega_0} = \frac{\mu(\gamma)}{\omega(\gamma)}, \quad (21)$$

$$\mu_1 = \frac{\sum_{i=\gamma+1}^L i p(i)}{\omega_1} = \frac{\mu_Y - \mu(\gamma)}{1 - \omega(\gamma)}, \quad (22)$$

where the total mean μ_Y of $\{Y_f\}_{f=1}^F$ is computed as

$$\mu_Y = \sum_{i=1}^L ip(i), \quad (23)$$

where $p(i)$ are the normalized frequencies (probabilities) corresponding to each bin i of the histogram.

The following relations have been readily verified in [35]:

$$\omega_0\mu_0 + \omega_1\mu_1 = \mu_Y \quad (24)$$

$$\omega_0 + \omega_1 = 1 \quad (25)$$

By considering (19) - (25) in (18), the between-class variance becomes

$$\sigma_b^2(\gamma) = \frac{[\mu_Y\omega(\gamma) - \mu(\gamma)]^2}{\omega(\gamma)[1 - \omega(\gamma)]} \quad (26)$$

Typically, the desired (optimal) threshold γ^* is the threshold that produces the maximum between-class variance computed in (26) over the total number of bins L . This is obtained as

$$\sigma_b^2(\gamma^*) = \max_{1 \leq \gamma \leq L} \sigma_b^2(\gamma) \quad (27)$$

Based on the constructs in (18) - (27), a new corollary can be obtained to determine the unimodality of an unknown distribution. First, we consider the following axiom: The between-class variance of a unimodal distribution does not exist, which is mathematically stated as: $\sigma_b^2(\gamma) = 0$. This axiom is obvious from Figure 2b - d where there exist no spatial separation between the classes in the different unimodal cases. Therefore, considering $\sigma_b^2(\gamma) = 0$ in (18), we obtain

$$\mu_0(\gamma) = \mu_1(\gamma), \quad (28)$$

Equation (28) is valid in the practical sense since all unimodal distributions are characterized by a single class. Consequently, it follows literally that the optimal threshold value γ^* obtained in (27) based on Otsu's

algorithm will yield $\sigma_b^2(\gamma^*) = 0$ for the unimodal case. Hence, (26) becomes

$$\mu_Y \omega(\gamma^*) = \mu(\gamma^*), \text{ for } \sigma_b^2(\gamma^*) = 0. \quad (29)$$

Thus, in order to keep (25) valid in the unimodal case, it follows that either of the below statements is true:

$$\{\omega_0 = 0, \omega_1 = 1\} \text{ or } \{\omega_0 = 1, \omega_1 = 0\}, \quad (30)$$

which means that $\omega(\gamma^*) = 0$ or 1 (recall (19)), thus implying that (29) becomes either of the following:

$$\mu(\gamma^*) = \mu_Y, \text{ for } \omega(\gamma^*) = 1 \quad (31)$$

$$\mu(\gamma^*) = 0, \text{ for } \omega(\gamma^*) = 0 \quad (32)$$

Here, (31) and (32) are easily considered to be two new corollaries with interesting consequences. First, (32) implies that the mean corresponding to the optimal threshold value of the measured sample is zero following the use of the Otsu's algorithm. This implication is unrealistic and impractical since every measured sample set must have a mean value. On the other hand, (31) implies that the mean corresponding to γ^* for a unimodal distribution is equal to the mean of the measured sample set. This implication provides a more practical consequence, which we state as follows:

"The optimal threshold value computed using the Otsu's algorithm for a set of measured sample values obtained from a unimodal distribution is equal to the total mean of the entire sample set."

Following this new corollary, we present the following steps of a simple and practical protocol to automatically determine a unimodal distribution from an unknown measured sample:

1. We assume that the input sample set is $\{Y_f\}_{f=1}^F$
2. Use Otsu's algorithm in [35] to obtain an optimal threshold γ^* for $\{Y_f\}_{f=1}^F$
3. Compute the mean of $\{Y_f\}_{f=1}^F$ as $\mu_Y = \frac{1}{F} \sum_{f=1}^F Y_f$.
4. If γ^* is equal to μ_Y , (i.e. $\gamma^* - \mu_Y \approx 0$), then $\{Y_f\}_{f=1}^F$ is a product of a unimodal distribution.
5. However, if $\gamma^* \gg \mu_Y$, then $\{Y_f\}_{f=1}^F$ may belong to either a bimodal or multimodal distribution. In this regard, the case for determining either bimodal or multimodal distributions is already well-known (see [35]).

To provide an insight into the physical parameters of the derived corollary, let us consider a special case where the measured PSD output from a spectrum analyser is denoted as Y_f . In this case, the spectrum analyser is assumed to have swept through several channels $f = 1, 2, 3, \dots, F$. The elements of the sensed sample are collated in step 1 of the protocol, which implies that processing begins after a single sweep of the target spectrum (or bandwidth) is completed. Then, Otsu's algorithm is applied in step 2 to $\{Y_f\}_{f=1}^F$ in order to obtain an optimal threshold γ^* . The mean of the sample μ_Y is computed in step 3, and comparison is conducted in step 4 between γ^* and μ_Y . Decision regarding unimodality or multimodality is made as in step 4 or step 5 of the protocol.

4.3. New Heuristic to select thresholds in Noise-only regimes

Following the new corollary in Section 4.2, we construct a new heuristic to determine whether a measured sample contains only noise elements or not. In this article, a heuristic algorithm is defined as an algorithm that finds a solution among a number of possible solutions, however, they may not be guaranteed to always find the best solution [36]. Thus, they are considered to provide approximate and not exact solutions. In our case, once determined to contain only noise elements, the heuristic then selects the element with the maximum value in the sample as the appropriate threshold value since this threshold value will lie at or above the noise level. Thus, this approach automatically tries to ensure that the NPAQM maintains a low P_{FA} rate. The advantage of our heuristic is that users no longer need to manually pre-adjust P_{FA} rates per changing spectra condition. Instead, our heuristic strives automatically to keep the P_{FA} rate as low as possible per input sample.

To achieve this, our heuristic measures the degree of closeness between the estimated threshold value, γ^{eff} , obtained using Algorithm 1 and the mean μ_Y of the entire ordered sample set (recall step 3 in Section 4.2). If the difference is smaller than 10 % of the entire sample range ($y_{(F)} - y_{(1)}$), and γ^{eff} is less than or equal to μ_Y , then our heuristic indicates that the measured sample contains only noise elements. The entire process is summarized in Algorithm 2. In this regard, we have conducted several preliminary experiments using different values ranging from 1 to 20 % and found no reduction in the false alarm rate of our heuristic under different noise-only conditions. Thus, it is not necessary to search larger percentage or the entire sample range since the probability of including actual signal elements may increase as one searches farther away from the edges of the spectrum, as well as noting that this may increase the processing time of the algorithm. Further, since our heuristic will only operate under the noise-only condition (following step 2

Algorithm 2: Heuristic Algorithm to determine thresholds in Noise-only regimes**Input:**

1. PSD elements, Y_f , for $f = 1, 2, \dots, F$
2. γ^{eff} obtained from Algorithm 1

Output: Final threshold value, γ^{eff}

```

1 Compute the mean of  $Y_f$  as  $\mu_Y = \frac{1}{F} \sum_{f=1}^F Y_f$ 
2 if  $[\gamma^{eff}] \leq [\mu_Y]$  then
3   if  $|\mu_Y - \gamma^{eff}| \leq 0.1 * [y_{(F)} - y_{(1)}]$  then
4      $\theta = 0.1 \times F$  //Obtain index of edge elements//
5      $\gamma^{eff} = \max \left[ \max_{f=1,2,\dots,\theta} (Y_f), \max_{f=F-\theta, F-\theta+1, \dots, F} (Y_f) \right]$ 
6   else
7      $\gamma^{eff} = \gamma^{eff}$  // $\gamma^{eff}$  is left unchanged//
8   end
9 else
10   $\gamma^{eff} = \gamma^{eff}$  // $\gamma^{eff}$  is left unchanged//
11 end

```

of Algorithm 2), thus, it is designed to find the maximum value within any percentage value of the total number of elements assigned by the user (following step 5 of Algorithm 2). Therefore, this implies that only higher threshold values will be selected even if larger percentage values were assigned by the user, thus further reducing the false alarm rate as desired in noise-only conditions. Consequently, searching through 10 % of the entire sample size ensures that, at least, part of the edges of the spectrum will be explored towards determining the maximum noise (peak) value that establishes an effective threshold value. For this reason, Algorithm 2 is only referred to as a heuristic. Nevertheless, sequel to performing the unimodality test via step 2 of Algorithm 2, the heuristic selects a final threshold value by examining the edge elements in Y_f where it is considered most probable to find noise elements. This assumption is further supported following the fact that the *shape factor* of typical bandpass filters is defined by responses that rise and fall at the spectra boundaries [37], where the smallest noise elements are most probable to be found. Consequently, our heuristic selects an appropriate γ^{eff} that corresponds to the maximum element value obtained from both tails of the power spectra.

Summarily, since every input sample will contain either only noise or a combination of signal-plus-noise elements, it becomes straightforward to deploy our methods as follows: In the case wherein the input sample comprises both signal-plus-noise elements (i.e the case for bimodality), Algorithm 1 operates effectively in

estimating a threshold value in this case. However, its performance may be limited by the signal-to-noise ratio and number of elements in the input sample. On the other hand, if the input sample contains only noise elements (i.e the unimodality case), this will be effectively determined by Algorithm 2 (the heuristic), which is based on the proposed test for unimodality. Essentially, our method works by sequentially executing the NPAQM (Algorithm 1) followed by Algorithm 2 in order to compute a useful threshold value for the effective detection of PU signals in a specific channel. We shall present results in Section 6 to demonstrate the effectiveness of our proposed methods.

4.4. Time Complexity Analysis of the NPAQM

We analyse the time complexity (TC) of the NPAQM as follows: We consider the number of machine instructions required to execute the NPAQM as a basis for approximating the TC. To achieve this, we remove all constant factors within the steps of the NPAQM to ensure that its running time scales according to the input sample size F , particularly as F tends to infinity. Similarly, we exclude lower order terms to asymptotically describe the TC [38]. Thus, we note that (6) - (17) are evaluated once in constant time reducing to steps of $\mathcal{O}(1)$. The NPAQM evaluates a *for* loop in steps 6 - 9 of Algorithm 1, thus having a TC of $\mathcal{O}(M)$, where $M \ll F$. The NPAQM reorders the input sample $\{Y_f\}_{f=1}^F$ in step 1 of Algorithm 1 based on a TC of $\mathcal{O}(F)$, which can be obtained using any of the best sorting algorithms, such as Timsort [39]. Without any other nested *for* loop in both Algorithms 1 and 2, and since $F \gg M$, the NPAQM approximates to an overall TC of $\mathcal{O}(F)$, which makes for a highly scalable and fast algorithm comparable to other well-known algorithms in the literature.

5. Empirical Method of Analysis

We analysed and compared the NPAQM against other methods using the empirically computed P_D and P_{FA} of each algorithm described statistically as

$$P_D = \Pr(Y_f > \gamma \mid H_1), \quad f = 1, 2, \dots, F \quad (33)$$

$$P_{FA} = \Pr(Y_f \geq \gamma \mid H_0), \quad f = 1, 2, \dots, F \quad (34)$$

where Y_f is the input PSD sample with each element located at a different frequency index $f = 1, 2, \dots, F$, and γ is the threshold value estimated by the algorithm.

We computed the receiver operating characteristic (ROC) curve (P_D vs P_{FA}) using Fawcett's empirical approach [40] as adapted in Figure 3. First, we labelled each input sample in a binary fashion to obtain the ground-truth of the different samples used in our simulations. By binary fashion, we refer to the labelling of zeroes and ones, where zeroes denote noise elements, whereas ones denote signal elements. The different samples used in our experiments are presented and discussed in Section 6. The ground-truth of each sample was obtained using an *a priori* known true threshold value (see Figure 3) corresponding to each respective sample. In this regard, the peak value of the noise floor in each sample was selected to be the true threshold value, which we defined based on the thermal noise floor of the simulated ED-based CR system. Thus, for the ground-truth of each sample, we considered the magnitude of each element above the true threshold value as a true signal element (and this was labelled as 1), whereas elements with magnitude below the true threshold value were considered as noise elements (and were labelled as 0). We used this binary procedure to obtain the ground-truth corresponding to each test sample.

Subsequently, we applied the same binary labelling procedure based on the actual threshold value estimated by the NPAQM and other algorithms in order to obtain the real outcome. Then, using the well-known confusion matrix [40], a missed detection is declared to have occurred if an algorithm labels an element as 0 instead of 1 as in the ground-truth (see Figure 3a). We declared a false alarm to have occurred if an algorithm labels an element as 1 instead of 0 as in the ground-truth (false positive (see Figure 3b)). Likewise, we declared a correct detection to have occurred if an algorithm correctly labels an element as 1 similar to the ground-truth (i.e. a true positive).

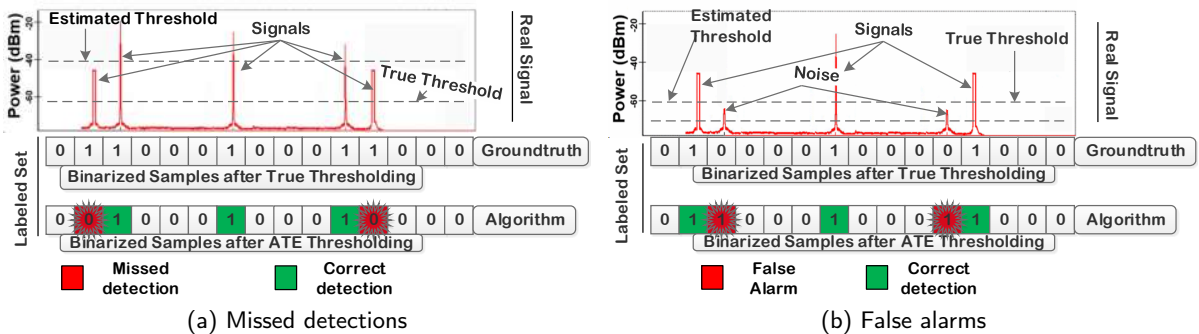


Figure 3: Method of Labelling and Analysis showing different errors [41]

Following the above, the P_D per sample was then computed as [40]:

$$P_D = \frac{\phi}{\rho}, \quad (35)$$

where ϕ denotes the total number of true positives (truly detected signal elements) if $Y_f > \gamma \mid H_1$, and ρ is the total number of actual true signal elements (obtained as the total number of ones in the ground-truth).

The P_{FA} per sample was computed as

$$P_{FA} = \frac{\varphi}{\eta}, \quad (36)$$

where φ denotes the total number of false positives (falsely detected signal elements) if $Y_f > \gamma \mid H_0$, and η is the total number of true noise elements (obtained as the total number of zeroes in the ground-truth). Our findings are reported in the next section.

6. Results and Discussion

We present and discuss our findings in two main subsections: first, we present results to validate the new corollary to automatically determine a unimodal distribution. Then we discuss our findings based on the performance of the NPAQM under different operating spectra conditions. In testing the NPAQM, first, we present results to validate our new heuristic algorithm under noise-only conditions and thereafter present our findings under different signal-plus-noise conditions. Our findings are discussed relative to the specification of the IEEE 802.22 standard for CR, which states that $P_D > 0.9$ and $P_{FA} < 0.1$ [42]. All simulations were conducted using MATLAB version R2017b and the entire samples used in our evaluation are made freely accessible in [43]. Importantly, since our research focuses on non-parametric SATAs, we compared the NPAQM with other non-parametric methods such as the methods in [19] and [9]. We note that Datla's approach in [19] is based strictly on the Otsu's method, so we shall refer to it simply as the Otsu's method, whereas the method in [9] is termed the modified-Otsu, which we term Mod-Otsu. It is noted also that the signal-to-noise ratio (SNR) considered in our experiments refers to the difference between the maximum magnitude of the signal element (in dB) and the maximum (peak) magnitude of the noise element (in dB) within a specified bandwidth. Such a difference is more or less related to the dynamic range of the input sample.

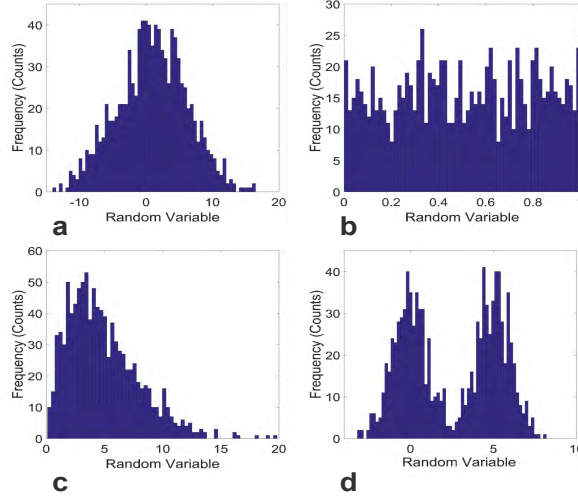


Figure 4: Different Sample Histograms: (a) Unimodal Gaussian Distribution, (b) Unimodal uniform Distribution, (c) Unimodal Chi-square Distribution, (d) Bimodal Gaussian Distribution

6.1. Tests to validate the New Corollary

In this section, three notable processes, including the Gaussian, uniform and Chi-square processes were considered to validate the new corollary. These processes were considered to analyse the response of our protocol to the effect of both symmetric (Gaussian and uniform) as well as asymmetric (Chi-square) distributions. The values in each table presented in this section were obtained by averaging over 1000 different Monte Carlo trials. In each table, the following metrics are presented and described as follows: $\{\mu_k\}_{k=1}^K$ denotes the theoretical mean used in the random number generator corresponding to each process (or distribution), μ_Y is the actual mean value computed from the randomly generated sample, and γ^* denotes the optimal threshold value estimated via the Otsu's algorithm. We used the independent t-test statistical measure to compare the actual mean and the mean of the estimated threshold values for samples generated via the different processes. The t-test was considered since it effectively determines whether the means of the two sets of data are significantly different from each other. The measure of statistical significance is stated per experiment based on the computed two-tailed P-value. In this regard, we tested our protocol using the Gaussian, uniform and Chi-square models provided in MATLAB (version R2017b) to generate random numbers corresponding to each distribution. The sample histograms corresponding to each distribution captured from one of several Monte Carlo trials are shown in Figure 4.

Table 1

The parameter values from a unimodal Gaussian Distribution over a fixed variance for a computed two-tailed P – value of 0.648 and t – test value of -0.0003

k	F	μ_k	μ_Y	γ^*
1	50	0.0000	0.0070	0.0080
2	100	1.0000	1.0010	1.0030
3	200	2.0000	2.0050	2.0020
4	300	3.0000	3.0040	3.0070
5	500	4.0000	4.0013	4.0013
6	1000	5.0000	5.0082	5.0068

6.1.1. For unimodal Gaussian Process

A set of random numbers $\{Y_f\}_{f=1}^F$ were generated based on the Gaussian distribution model over different sample sizes F using different theoretical mean values $\{\mu_k\}_{k=1}^K$, for $K = 6$, and using a fixed variance of $\sigma^2 = 5$ for each k . In this case, the following set of theoretical mean values were used $\mu_k = \{0, 1, 2, 3, 4, 5\}$. Subsequently, 1000 Monte Carlo trials were conducted in order to arrive at an average value for both μ_Y and γ^* . The results obtained are presented in Table 1.

While it may be straightforward to observe (in Table 1) that the values of μ_Y and γ^* are approximately the same, nevertheless, for a computed two-tailed P – value of 0.648 and a t – test value of -0.0003, it is noted that there is not a statistically significant difference between the values of μ_Y and γ^* , respectively. The new test is shown to be further valid under different sample sizes as shown in Table 1. In this case, both the distribution's mean μ_k and the sample sizes F were varied simultaneously and the values of μ_Y and γ^* remained approximately equal (i.e. $\mu_Y - \gamma^* \approx 0$). Consequently, the results in Table 1 confirm that the theoretical corollary of (31) is valid for the case of the unimodal Gaussian distribution.

6.1.2. For unimodal uniform Process

A similar procedure as above was carried out to test the case of a uniform unimodal process. Uniformly distributed random numbers were generated over the range $[u_1, u_2]$. In this case, the lower range μ_1 was fixed at $u_1 = 0$, while the upper range u_2 of the distribution was varied. We then subjected these uniformly generated samples to the new protocol of the corollary. The results obtained are provided in Table 2.

We show in Table 2 that both μ_Y and γ^* have very close values, which validates the theoretical conclusion of the new corollary in (31) for the uniform unimodal process based on a t-test value of -0.0002 and a two-tailed P-value of 0.999846.

Table 2

The parameter values for the unimodal uniform Distribution for a computed two-tailed $P - value$ of 0.999846 and $t - test$ value of -0.0002

u_2	μ_Y	γ^*
5.0000	2.4998	2.5008
10.0000	4.9972	4.9973
15.0000	7.5000	7.4975
20.0000	9.9987	9.9985
25.0000	12.4952	12.4940
30.0000	14.9815	14.9875

Table 3

The parameter values for the unimodal Chi-square Distribution for a computed two-tailed $P - value$ of 0.95 and $t - test$ value of -0.347

V	μ_Y	γ^*
5.0000	5.0031	5.1752
10.0000	9.9939	10.1839
15.0000	14.9893	15.1783
20.0000	20.0048	21.1805
25.0000	24.9928	25.1654
30.0000	29.9882	30.1688

6.1.3. For unimodal Chi-square Process

We tested the new corollary using Chi-square randomly generated numbers based on different degrees of freedom V . These randomly generated samples were subjected to our new protocol over 1000 Monte Carlo trials to validate the protocol. The results obtained are presented in Table 3 showing again that the values of μ_Y and γ^* are approximately equal (Table 3). To confirm this, we computed a two-tailed $P - value$ of 0.95, and a $t - test$ score of -0.347 with 10 degrees of freedom, which confirms that there is not a statistically significant difference between μ_Y and γ^* in Table 3. Thus, we have demonstrated further that the new corollary (see 31) is valid for the case of an asymmetric distribution such as the Chi-square distribution.

6.1.4. For Bimodal Gaussian Process

To further validate the new corollary, we demonstrate that it works only for unimodal distributions and not for bimodal distributions. To achieve this, we subjected our new protocol to samples from a bimodal distribution to ascertain its validity. In this test, we generated two normal distributions having the same variance ($\sigma^2 = 1$) but with different mean values of $\mu_1 = \{0, 1, 2, 3, 4, 5\}$ and $\mu_2 = \{10, 13, 15, 16, 19, 20\}$, respectively. Here, μ_1 is the mean value of the first distribution while μ_2 is the mean value of the second distribution. Although these mean values were chosen arbitrarily, however, they can be changed without necessarily affecting the validity of our test. Figure 4d shows a capture of the histogram of the bimodal sam-

Table 4

The parameter values for the Bimodal Gaussian Distribution for a computed two-tailed P – value of 0.034 and t – test value of 2.34

μ_1	μ_2	μ_Y	γ^*
0.0000	10.0000	5.0013	3.1082
1.0000	13.0000	6.9998	4.1053
2.0000	15.0000	8.5001	5.1050
3.0000	16.0000	9.4995	6.1219
4.0000	19.0000	11.4997	7.1261
5.0000	20.0000	12.4988	8.1261

ple drawn from within the Monte Carlo trials used to validate our protocol. Numerical results are presented in Table 4 to validate our test protocol.

Based on a computed two-tailed P – value of 0.034 and a t – test score of 2.463, there exists a statistically significant difference between μ_Y and γ^* , implying that the protocol fails under the bimodal case. This confirms that our new protocol is valid only for the test of unimodality, which makes it quite useful for detecting noise-only sample sets automatically. We shall show in the next subsection the usefulness of our new corollary under practical CR conditions using the heuristic in Algorithm 2.

6.2. Tests to validate the NPAQM's Performance

6.2.1. Under Noise-only conditions: The H_0 case

The NPAQM was tested considering three different noise-only sample sets. First, we considered samples of additive white Gaussian noise (AWGN) under two different sample lengths of $F = 250$ and 515 elements, respectively. The shorter sample length ($F = 250$) describes the case in which a CR system performs fast spectrum sensing, whereas the longer sample length ($F = 515$) corresponds to longer spectrum sensing time. Both conditions typically aid to investigate whether the performance of the NPAQM will be affected by sample length or not. Second, the NPAQM was tested under coloured noise conditions (precisely *pink* noise condition). This condition may arise when a CR system senses very wide bands, which is a possibility under real-life conditions. Thirdly, we considered the performance of the NPAQM under different noise uncertainty levels, which typically arise in practice. In all these conditions, we compared the NPAQM against two well-known non-parametric methods published in [9, 19].

In Figures 5a, 5c, and 5e, we present the actual sensed spectra graphs as measured by the simulated ED-based CR system and the respective threshold values (see lines) estimated by the different algorithms. Figure 5a presents the spectra of an AWGN sample with dimension $F = 250$ elements. Here, we mention

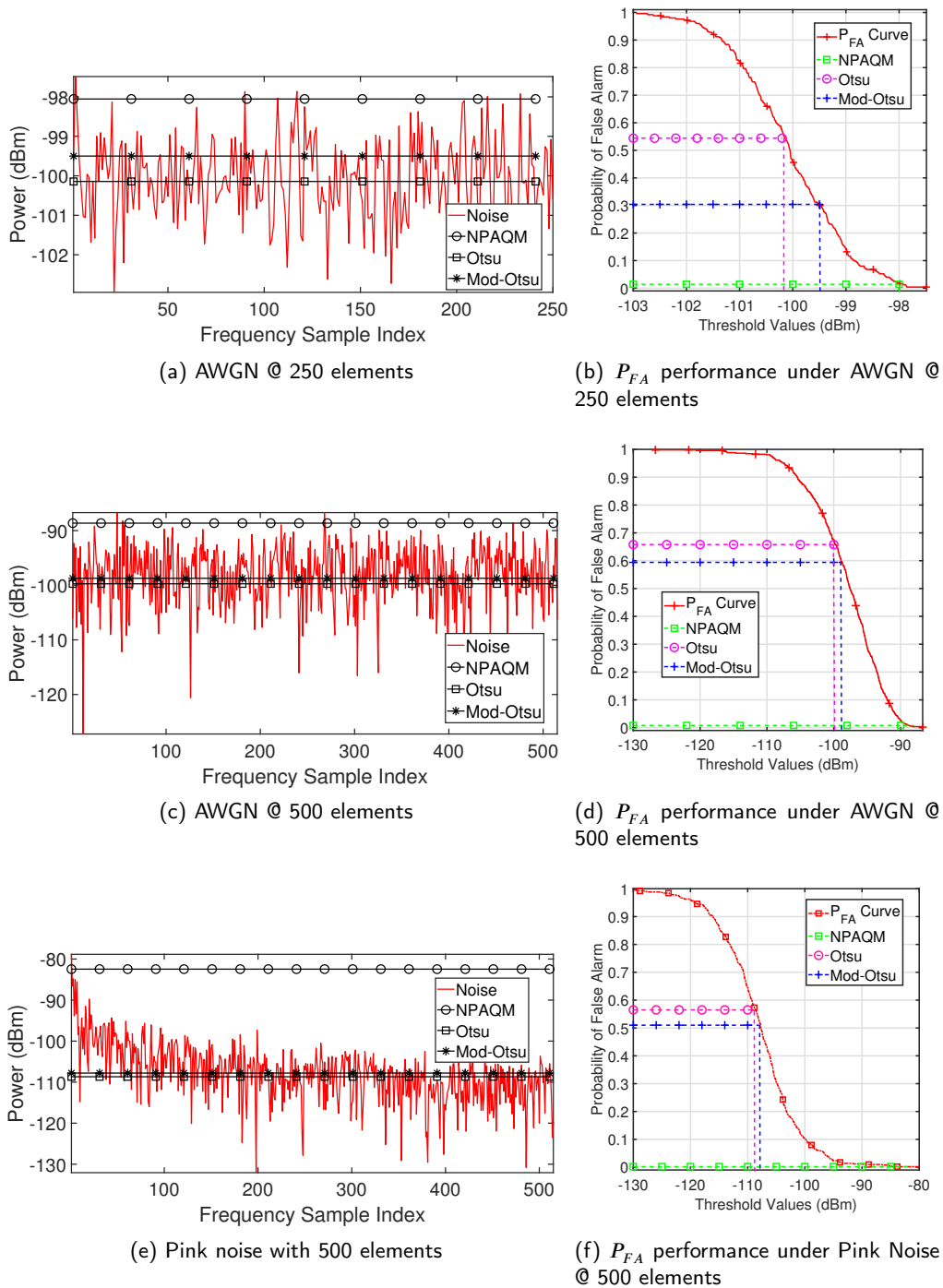


Figure 5: Estimated thresholds of each technique over different noise characteristics and sample lengths and the corresponding false alarm performance of each technique

that the ground-truth threshold value required to maintain a minimum P_{FA} rate of $P_{FA} = 0.01$ is -97.5 dBm. Interestingly, the NPAQM estimated autonomously a threshold value of -98 dBm, which produced

Table 5 P_{FA} rate (in percentage) under different noise uncertainty levels in AWGN

Noise Uncertainty (dB)	P_{FA} (in %)		
	NPAQM	Otsu [19]	Mod-Otsu [9]
1	0.4	50.0	30.8
3	0.4	61.6	34.8
5	1.6	54.4	38.0

$P_{FA} = 0.02$ as shown in the corresponding performance curve of Figure 5b. It is seen in Figure 5b that the NPAQM achieved the least P_{FA} rate as against the other methods owing to the capability of our heuristic (see Algorithm 2) to identify such noise-only conditions in order to minimize the P_{FA} rate of the NPAQM. This further validates the practical potentials of the new corollary described in Section 4.2 since our heuristic was built upon the proposed corollary. Consequently, the NPAQM was able to select the element with the maximum value from both ends of the spectra towards producing the lowest achievable P_{FA} rate as against the other methods.

Then, we increased the dimension of the noise sample from 250 to 515 elements and re-examined the performance of the different algorithms. The spectra and the respective threshold values estimated by the different algorithms are graphed in Figure 5c. In the corresponding performance graph of Figure 5d, the NPAQM is shown to produce a minimum P_{FA} rate of $P_{FA} = 0.02$ based on an estimated threshold value of -89.6 dBm (see Figure 5c). In this case, it is seen in Figure 5d that the Otsu [19] and Mod-Otsu [9] methods produced very high P_{FA} rates since they are unable to determine the present condition as comprising noise-only elements. Consequently, both methods placed their threshold values approximately mid-way through the spectra, which led to considerably high P_{FA} rates. Again, the NPAQM outperformed these other methods because it engaged the improved capability of the heuristic algorithm deployed to autonomously minimize its P_{FA} rate. Interestingly, since the NPAQM would always attempt to select the maximum value under noise-only conditions, it is thus able to achieve the minimum P_{FA} rates typically specified by the IEEE 802.22 standard, hence making it a dependable algorithm under practical conditions.

We tested the NPAQM further under the *pink* noise condition (using a sample length of 515 elements) with the spectra as shown in Figure 5e. Here, Figure 5e confirms the presence of *pink* noise characteristics since the energy level is seen to slowly ramp downwards from the left to the right side of the spectra, which indicates the presence of lower noise values at higher frequencies as expected under *pink* noise conditions. In this case, the NPAQM achieved the lowest P_{FA} rate of $P_{FA} = 0.0019$ as shown in Figure 5f. The NPAQM

performed well because it applied the new heuristic of Algorithm 2, which ensured that higher threshold values were selected in order to minimize the algorithm's P_{FA} rate automatically. Again, the Otsu and Mod-Otsu methods both performed poorly under this condition since they lack such effective methods to minimize their respective P_{FA} rates.

Further, we investigated the performance of the NPAQM under different noise uncertainty levels as obtained under real practical CR conditions. We varied the noise uncertainty levels in steps of 1, 3, and 5 dB, respectively and the results obtained are presented in Table 5. Here, we show that the NPAQM achieved the lowest P_{FA} rate under all uncertainty conditions. It is worth mentioning that we have presented only P_{FA} results in this subsection since there exist no signal elements to be detected. Summarily, the NPAQM is shown to have performed best under the different noise-only conditions of this section owing to the capability of Algorithm 2, which is based on the validity and effectiveness of the newly proposed corollary of Section 4.2. We note that since Algorithm 2 exists independently of Algorithm 1, thus, Algorithm 2 can be used by other methods including the Otsu and Mod-Otsu methods as well as other regular ATAs in order to minimize their P_{FA} rates under such noise-only conditions. This is an interesting conclusion from our findings, which not only establishes the NPAQM as an effective algorithm, but also establishes Algorithm 2 as an effective extension deployable in other methods.

6.2.2. Under Signal-plus-Noise conditions: The H_1 case

The NPAQM was tested under different signal-plus-noise conditions. First, effort is made to determine the minimum SNR level below which the performance of the NPAQM may no longer be guaranteed. In order to achieve this, we examined the case of detecting both frequency modulated (FM) carrier and orthogonal frequency division multiplexing (OFDM) signals. We considered FM carrier signals for the case wherein a CR system may need to detect existing microphone signals within a regular TV band, whereas OFDM signals were considered in order to investigate the possible case of detecting digital television (DTV) signals. Further in this section, we tested each algorithm under both narrow and wideband sensing conditions as well as under the Rayleigh fading case. We also considered a broad range of SNR values from 5dB to 25 dB under Rayleigh fading conditions. This range is typically sufficient since radio systems are often required to detect as high as 20dB in some data network applications and 25 dB in some voice applications. Thus, a CR device should be able to detect high SNR levels, as well as very low levels, particularly towards the 0 dB level. We present our findings as follows:

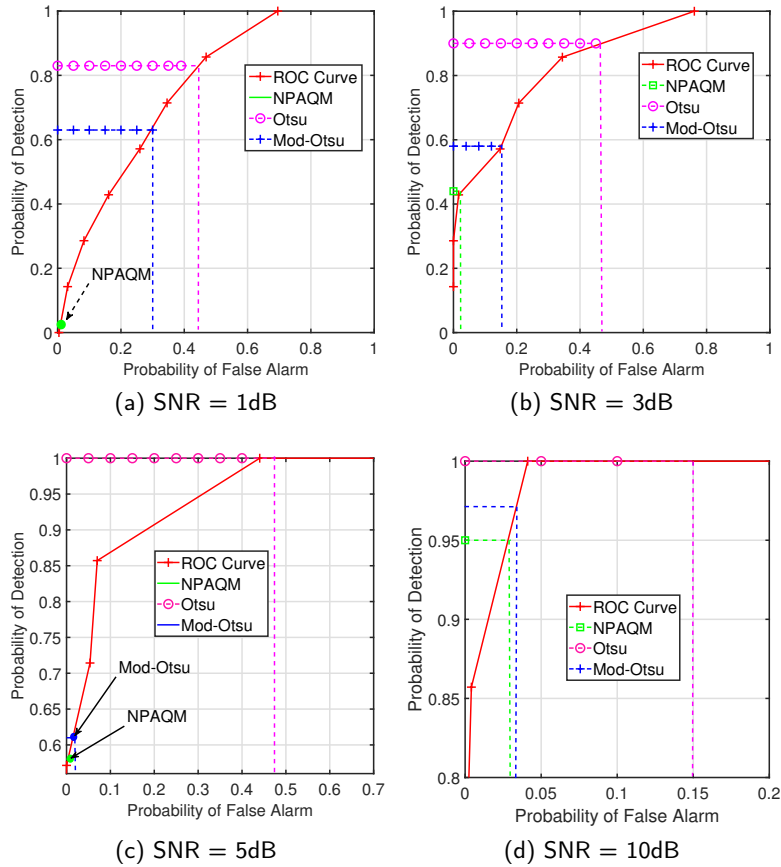


Figure 6: For FM Carrier signal: ROC curves showing the performance of the different techniques at different SNR levels

6.2.2.1. *Using FM signal* The receiver operating characteristic (ROC) curves obtained for detecting the FM carrier signal under different SNR values are shown in Figures 6a - 6d. In this case, the sample length of the dataset was fixed at 250 elements. It should be noted that towards computing the different ROC performance curves of Figure 6, we note that the actual signal elements were located from the 80th - 90th element, whereas all other elements were purely noise-only elements as shown in the corresponding spectra graphs of Appendix B. In Appendix B, we present the respective spectra graphs used to obtain the corresponding ROC curves of Figure 6 at the different SNR levels, respectively.

In Figure 6a, it can be observed that the NPAQM achieved the lowest P_{FA} under the $SNR = 1dB$ condition albeit at the expense of a corresponding low P_D rate. This performance is expected since signals at such low SNR levels would typically be indistinguishable from noise. Interestingly, instead of increasing its P_{FA} rate in order to increase its P_D rate, the NPAQM remarkably opted to maintain a low $P_{FA} = 0.004$

rate since it was able to determine that this case comprised noise-only elements based on the use of Algorithm 2. On the other hand, the Otsu and Mod-Otsu methods opted instead to maximize their P_D rates albeit at very high P_{FA} rates (see Figure 6a). Such very high P_{FA} rates of the Otsu and Mod-Otsu methods would definitely be detrimental to CR networks since much of the spectrum will be left underutilized.

Under the higher SNR levels of Figures 6b - 6d, it can be seen that the NPAQM gradually increased its P_D rate while strongly ensuring that its P_{FA} rate was kept as low as possible. Notably, the NPAQM achieved a maximum P_D rate of $P_D > 0.9$ at the $SNR = 10dB$ level while guaranteeing $P_{FA} < 0.1$. This cannot be said of the Otsu and Mod-Otsu methods, which are seen to incur very high P_{FA} rates even at higher SNR levels. An exception can be observed for the Mod-Otsu method at the $SNR = 10dB$ level, wherein a stable performance of $P_D > 0.9$ and $P_{FA} < 0.1$ was achieved. Consequently, it can be concluded that the NPAQM achieves a better well-behaved performance as against the other methods in terms of minimizing its P_{FA} rate, while an appreciable detection performance can be guaranteed when $SNR \geq 10dB$.

6.2.2.2. Using OFDM signal The performance curves corresponding to the detection of OFDM signals are shown in Figures 7a - 7d. Again we note that the corresponding spectra graphs used to compute the respective ROC curves at different SNR levels are presented in Appendix C. In this case, it is worth noting that a large sample length of $F = 4096$ was used, thus making the empirically computed ROC curves much smoother than in the FM case. In computing the ROC curves, we note that the actual signal elements in Figures 11a - 11d of Appendix C were located from the 300th to 3800th element index, whereas all other elements were purely noise-only elements.

Similar to the FM case, it can be observed in Figure 7a that the NPAQM achieved the lowest P_{FA} rate in the $SNR = 1dB$ case. In particular, the NPAQM selected a very high threshold value in this case based on the use of Algorithm 2, which led to such a low P_{FA} rate. This performance can be explained by considering the fact that the OFDM signal assumes a noise-like characteristics, particularly at its crest, thus leading the NPAQM to consider the sample as comprising noise-only elements. However, the performance of the NPAQM can be seen in Figures 7b - 7d to have greatly improved, particularly at $SNR > 5dB$, thus satisfying the IEEE 802.22 standard. It can be deduced from our findings that, it is easier to detect OFDM signals as against detecting only the carrier of an FM signal. This can be explained considering the effect of occupancy since the FM carrier signal occupies a relatively narrower bandwidth as against the OFDM signal. This may indicate that both the width as well as the magnitude of a PU signal may greatly affect the

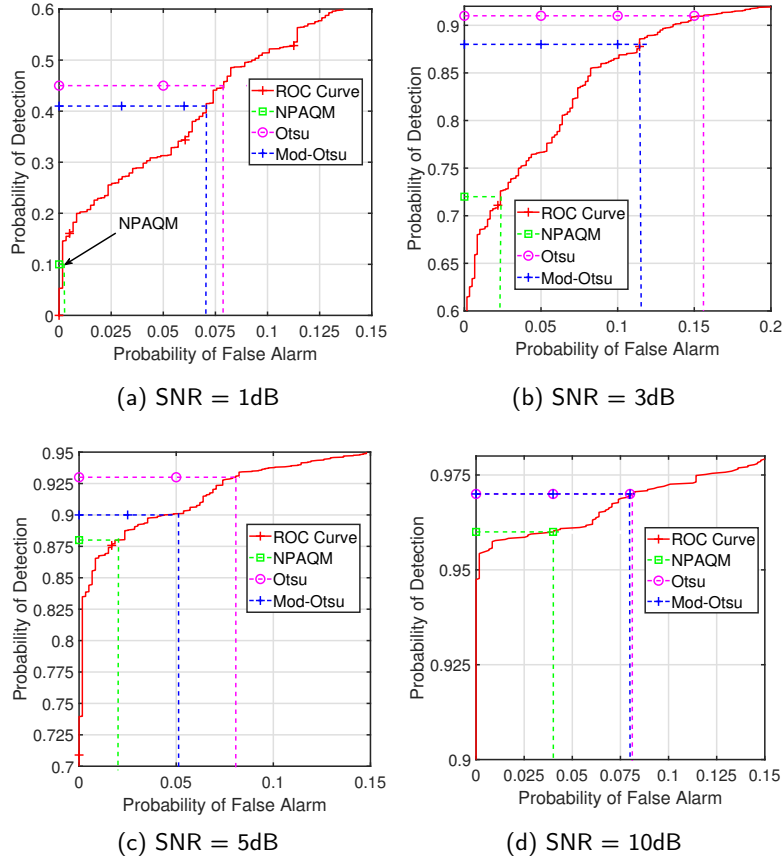


Figure 7: For OFDM signals: ROC curves showing the performance of the different techniques at different SNR levels

detection performance of typical threshold adjustment algorithms. Consequently, we further explore these observations in greater details in the next subsection.

6.2.2.3. Under narrow and wideband sensing conditions The spectra graphs for the case of narrow and wideband sensing are shown in Figures 8a and 8c, whereas their corresponding performance curves are presented in Figures 8b and 8d, respectively. In occupancy terms, the narrowband signal mimics the case of a highly occupied band since the signal can be seen to occupy most of the spectrum from the 40th to 220th element (see Figure 8a). The narrowband condition is a worthwhile and often difficult case to select accurate threshold values because a larger portion of the band may belong to signal elements, thus approximating a unimodal distribution (recall Figure 2 in Section 4.2). Nevertheless, it is seen in Figures 8b and 8d that the NPAQM performed better than the Otsu and Mod-Otsu methods by yielding $P_D = 0.97$ at $P_{FA} = 0.075$ for the narrowband case and $P_D = 0.91$ at $P_{FA} = 0.03$ for the wideband case.

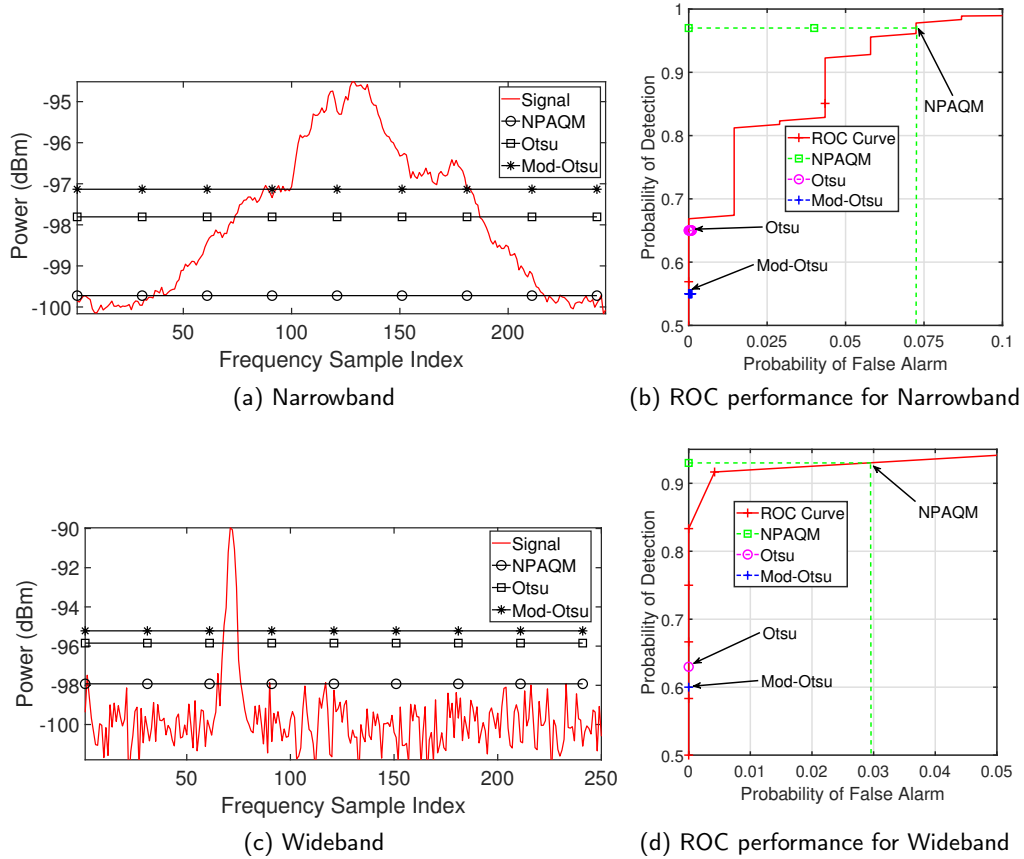


Figure 8: Estimated thresholds over different sensed bands (a) Narrowband (b) Wideband

For the case of wideband sensing (i.e low/sparse occupancy), the signal elements occupied about 8% of the entire bandwidth (i.e from the 60th - 80th element). By using a high enough SNR level (i.e. $SNR = 8dB$) in this case, the signal was well detected by the NPAQM in the wideband case as compared to the Otsu and Mod-Otsu methods. This can be attributed to the use of the first order difference function in the NPAQM, which ensured that a better defined boundary was accurately detected between the noise and signal elements in the input sample. The Otsu and Mod-Otsu algorithms may have achieved lower P_{FA} rates in both cases, but this is because both the narrow and wideband datasets were designed to approximate unimodal distributions. Such effects of unimodality made both algorithms to place their thresholds about mid-way through the magnitude of the input sample leading to lower P_{FA} rates. The narrowband case approximates a unimodal distribution since it contains over 90% of signal elements, whereas the wideband case approximates a unimodal distribution since it contains over 90% of noise-only elements.

In this regard, the NPAQM maintained an appreciable and balanced performance as against the other

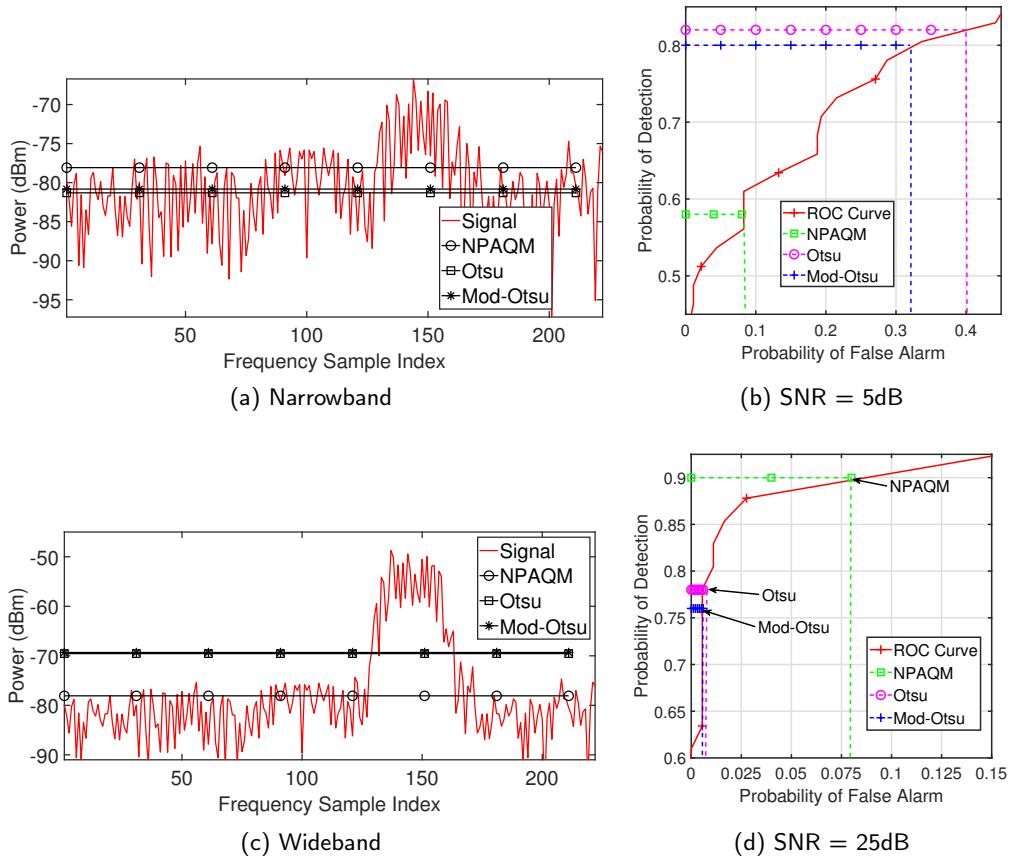


Figure 9: Estimated thresholds over Rayleigh fading spectra and the corresponding ROC performance curve showing the performance of the different techniques. The displays of the raw spectra data for the narrow and wideband signals are shown in (a) and (c), respectively, whereas the corresponding ROC curves obtained for the different spectra data are shown in (b) and (d) at the different SNR levels.

methods because it adopts Algorithm 2, which opts to inspect the spectra edges whenever the case for unimodality is detected. Technically, this ensures that the NPAQM maintains a good performance level independent of the size of the sensed bandwidth, thus making it viable for use in practice.

6.2.2.4. Under Rayleigh Fading conditions The NPAQM was tested further considering the case of Rayleigh fading channels. We considered two different Rayleigh fading channels with $SNR = 5dB$ and $25dB$, respectively. These were generated at a sample rate of 9600 Hz and a Doppler frequency of 100 Hz. Figure 9a graphs the spectra in the low SNR case showing the selected thresholds, whereas Figure 9b presents the corresponding ROC performance curve of the low SNR case. In both Figures 9a and 9c, the signal elements are designed to exist between the 125th - 170th element in both cases, whereas all other elements are purely noise-only elements. In the low $SNR = 5dB$ case, the NPAQM is shown in Figure 9b to achieve $P_D = 0.58$

at $P_{FA} = 0.008$, which demonstrates that yet again the NPAQM maintains a very low P_{FA} rate even under fading channels at low SNR levels albeit at a low P_D rate.

We increased the SNR level (see Figure 9c) and the NPAQM is again shown to maintain a high P_D rate albeit at a slightly higher P_{FA} rate (i.e. $P_{FA} = 0.08$), which remains within the requirement of the IEEE 802.22 standard i.e. $P_{FA} < 0.1$. Most interestingly, we note that the P_{FA} rate of our method does not continue to grow with an increase in the SNR level, instead it asymptotically converges to below the $P_{FA} = 0.1$ rate as stipulated by IEEE 802.22 standard for CR. This is confirmed based on the results obtained at very high SNR levels of 25 dB as presented in Figure 9d. Here, our algorithm maintains a low P_{FA} rate even at very high SNR levels. Although it is appealing to design the P_{FA} and P_D rates to satisfy specific constraints, nevertheless, such designs may only suffice under conditions where the assumed noise distribution corresponds to the actual probability distribution of the real input signal. However, since this cannot be guaranteed at all times under all working conditions (see [13]), thus, SATAs such as our proposed NPAQM will be of great benefit to a number of signal detection conditions in CR applications.

7. Conclusion

In this article, a fully autonomous method is proposed called the non-parametric amplitude quantization method (NPAQM) for improving threshold estimation in ED-based CR systems. Different from existing approaches, the NPAQM does not require gray-scale computations or the generation of histograms as required in existing methods, thus guaranteeing faster processing times based on a time complexity of $\mathcal{O}(F)$, where F is the total number of input elements. Furthermore, we have presented a new corollary to determine the unimodality of an unknown distribution, which can be applied to not only signal detection in CR, but to other statistical-based signal-processing applications such as in clustering, machine learning, modal determination problems, to name but a few. Following the new corollary, we have constructed a novel heuristic algorithm to improve the performance of the NPAQM and possibly other methods under noise-only regimes. Our heuristic algorithm ensures that the NPAQM maintains an acceptable P_{FA} rate (i.e. $P_{FA} < 0.02$) under different dynamic spectra conditions. The NPAQM is notably independent of the size of the sensed bandwidth since it performs well under both narrow and wideband sensing conditions. In general, our algorithm performed better in P_{FA} terms than the other non-parametric methods compared with in the present article. Specifically, in the noise-only regime, the NPAQM achieved about 96.36 % and 95 % decrease in the P_{FA}

rate as compared to the Otsu and Mod-Otsu methods, respectively. This lower P_{FA} rate was maintained by our algorithm even under low SNR conditions (i.e. SNR < 5 dB) albeit at a lower P_D rate as compared to the other methods. However, at higher SNR levels (i.e. SNR > 5 dB), the NPAQM achieved similar to the other methods a high P_D rate ($P_D > 0.9$) while still maintaining a lower P_{FA} rate than the Otsu and Mod-Otsu methods. In future works, the P_D rate of the NPAQM will be improved particularly at such lower SNR levels (SNR < 3 dB) to further reduce the probability of interference with existing PU transceivers. Presently, our findings suggest that the NPAQM provides an improved performance as against other fully autonomous methods, thus emphasizing its potentials for use in self-reconfigurable CR systems.

A. Appendix-A

Equation (5) in the main text is derived in this section. Let the FFT length F used to compute the frequency response of the input signal $y(t)$ be defined as

$$F = 2^x, \quad (37)$$

where x is the next power of 2, which is to be computed from the input signal length N . However, since the new length F may contain trailing zeros, which pad the input signal in order to improve the FFT's performance, thus, it is required that

$$2^x > N - 1, \quad (38)$$

where N is obtained as $N = T_s \times f_s$, and T_s is the sensing period whereas f_s is the sampling frequency. Note that the number of FFT points goes from 0, 1, ..., $N - 1$, which accounts for the use of $N - 1$ in (38). Thus, from (38), x is obtained as

$$x > \log_2(T_s \times f_s - 1) \quad (39)$$

Substituting (39) in (37) yields the new FFT length as

$$F = 2^{\lceil \log_2(T_s \times f_s - 1) \rceil} \quad (40)$$

The ceiling notation is introduced in (40) so that x is made always greater than $\log_2(T_s \times f_s - 1)$ towards ensuring that the input signal length is properly zero padded.

B. Appendix-B

The spectra graphs presented in Figures 10a - 10d are the datasets used to compute the corresponding ROC curves presented in Figures 6a - 6d at different SNR levels, respectively.

C. Appendix-C

The spectra graphs presented in Figures 11a - 11d are the datasets used to compute the corresponding ROC curves presented in Figures 7a - 7d at different SNR levels, respectively.

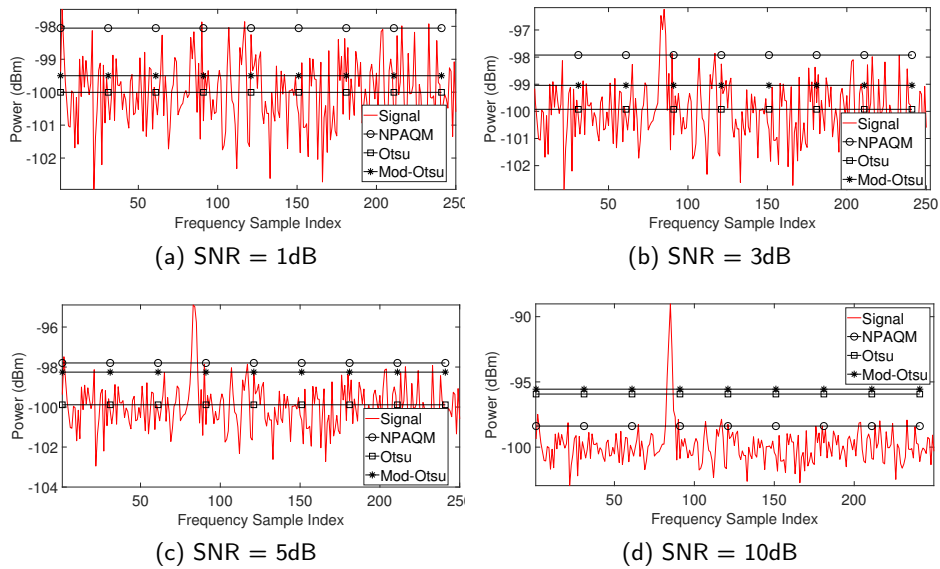


Figure 10: For FM Carrier signal: The actual spectra graphs showing the different threshold values estimated by the different techniques under different SNR levels

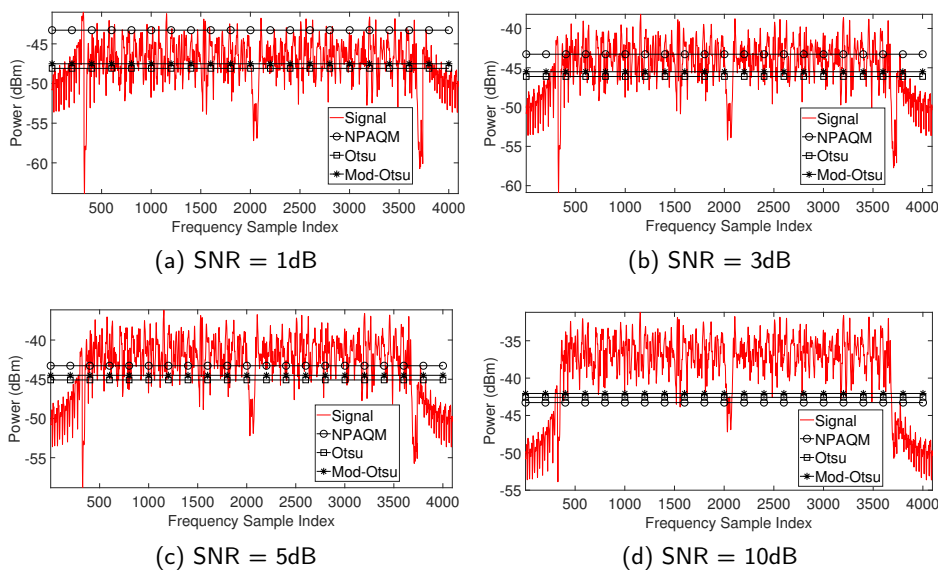


Figure 11: For OFDM signals: The actual spectra graphs showing the different threshold values estimated by the different techniques under different SNR levels

References

- [1] T. Yucek and H. Arslan, "A survey of spectrum sensing algorithms for cognitive radio applications," *IEEE communications surveys & tutorials*, vol. 11, no. 1, pp. 116–130, 2009.
- [2] I. F. Akyildiz, W. Y. Lee, M. C. Vuran, and S. Mohanty, "NeXt generation/dynamic spectrum access/cognitive radio wireless networks: A survey," *Computer Networks*, vol. 50, pp. 2127–2159, 2006.
- [3] A. J. Onumanyi, A. M. Abu-Mahfouz, and G. P. Hancke, "Cognitive radio in low power wide area network for IoT applications: Recent approaches, benefits and challenges," *IEEE Transactions on Industrial Informatics*, pp. 1–9, Nov. 2019. DOI: 10.1109/TII.2019.2956507.
- [4] H. M. Farag and E. M. Mohamed, "Soft decision cooperative spectrum sensing with noise uncertainty reduction," *Pervasive and Mobile*

- Computing*, vol. 35, pp. 146–164, 2017.
- [5] I. Mustapha, B. M. Ali, A. Sali, M. F. A. Rased, and H. Mohamad, “An energy efficient reinforcement learning based cooperative channel sensing for cognitive radio sensor networks,” *Pervasive and Mobile Computing*, vol. 35, pp. 165–184, 2017.
 - [6] S. R. Sabuj and M. Hamamura, “Outage and energy-efficiency analysis of cognitive radio networks: A stochastic approach to transmit antenna selection,” *Pervasive and Mobile Computing*, vol. 42, pp. 444–469, 2017.
 - [7] R. Vuohtoniemi, J. J. Lehtomäki, and J. P. Mäkelä, “Adaptive threshold based frequency exclusion algorithm for broadband {PLC},” in *2016 International Symposium on Power Line Communications and its Applications (ISPLC)*, IEEE, mar 2016.
 - [8] A. J. Onumanyi, A. M. Abu-Mahfouz, and G. P. Hancke, “Histogram partitioning algorithms for adaptive and autonomous threshold estimation in cognitive radio-based industrial wireless sensor networks,” *Transactions on Emerging Telecommunications Technologies*, pp. 1–15, 2019.
 - [9] A. J. Onumanyi, E. N. Onwuka, A. M. Aibinu, O. C. Ugweje, and M. J. E. Salami, “A modified Otsu’s algorithm for improving the performance of the energy detector in cognitive radio,” *AEU-International Journal of Electronics and Communications*, vol. 79, pp. 53–63, Sept. 2017.
 - [10] E. U. Ogbodo, D. Dorrell, and A. M. Abu-Mahfouz, “Cognitive Radio Based Sensor Network in Smart Grid: Architectures, Applications and Communication Technologies,” *IEEE Access*, vol. 5, no. c, pp. 19084–19098, 2017.
 - [11] J. Vartiainen, R. Vuohtoniemi, A. Taparugssanagorn, and N. Promsuk, “Interference suppression and signal detection for LTE and WLAN signals in cognitive radio applications,” *International Journal on Advances in Telecommunications*, vol. 10, no. 1-2, pp. 1–10, 2017.
 - [12] G. Celik, A. Aitalieva, H. Celebi, and M. Uysal, “A software defined radio based data link design for vhf band wireless sensor networks,” *Physical Communication*, vol. 30, pp. 167–178, 2018.
 - [13] J. D. Gibson and J. L. Melsa, *Introduction to nonparametric detection with applications*, vol. 119. Academic Press, 1976.
 - [14] A. J. Onumanyi, A. M. Abu-Mahfouz, and G. P. Hancke, “Adaptive threshold techniques for cognitive radio-based low power wide area network,” *Transactions on Emerging Telecommunications Technologies*, vol. 31, pp. 1–14, Feb. 2020. DOI: <https://doi.org/10.1002/ett.3908>.
 - [15] A. M. Abu-Mahfouz and G. P. Hancke, “ns-2 extension to simulate localization system in wireless sensor networks,” in *IEEE Africon’11*, pp. 1–7, IEEE, 2011.
 - [16] D. D. Olatinwo, A. M. Abu-Mahfouz, and G. P. Hancke, “A survey on LPWAN technologies in WBAN for remote health-care monitoring,” *Sensors*, vol. 19, no. 23, p. 5268, 2019.
 - [17] J. J. Lehtomäki, R. Vuohtoniemi, K. Umabayashi, and J. P. Mäkelä, “Energy detection based estimation of channel occupancy rate with adaptive noise estimation,” *IEICE transactions on communications*, vol. E95-B, no. 4, pp. 1076–1084, 2012.
 - [18] J. J. Lehtomäki, R. Vuohtoniemi, and K. Umabayashi, “Duty Cycle and Channel Occupancy Rate Estimation with MED-FCME LAD ACC,” in *Proceedings of the 7th International Conference on Cognitive Radio Oriented Wireless Networks*, vol. 248454, pp. 236–241, IEEE, 2012.
 - [19] D. Datla, A. M. Wyglinski, and G. Minden, “A spectrum surveying framework for dynamic spectrum access networks,” *IEEE Transactions on Vehicular Technology*, vol. 58, no. 8, pp. 4158–4168, 2009.
 - [20] A. Gorcin, K. A. Qaraqe, H. Celebi, and H. Arslan, “An adaptive threshold method for spectrum sensing in multi-channel cognitive radio networks,” *17th IEEE International Conference on Telecommunications (ICT)*, pp. 425–429, 2010.
 - [21] S. D. Barnes, P. J. Van Vuuren, and B. T. Maharaj, “Spectrum occupancy investigation: Measurements in South Africa,” *Measurement*, vol. 46, pp. 3098–3112, Nov. 2013.
 - [22] S. Koley and D. Mitra, “Edge-Fitting Based Energy Detection for Cognitive Radios,” *Journal of Signal Processing Systems*, dec 2017.
 - [23] K. Berbra, M. Barkat, F. Gini, M. Greco, and P. Stinco, “A fast spectrum sensing for CP-OFDM cognitive radio based on adaptive thresholding,” *Signal Processing*, vol. 128, pp. 252–261, 2016.
 - [24] J. Avila and K. Thenmozhi, “Adaptive double threshold with multiple energy detection technique in cognitive radio,” *Research Journal of Applied Sciences, Engineering and Technology*, vol. 10, no. 11, pp. 1336–1342, 2015.
 - [25] A. Bagwari and G. S. Tomar, “Two-stage detectors with multiple energy detectors and adaptive double threshold in cognitive radio networks,” *International Journal of Distributed Sensor Networks*, vol. 2013, 2013.
 - [26] B. Ahuja, K. Sharma, M. Abo-Zahhad, O. Amin, M. Farrag, A. Ali, and A. Rachman, “Adaptive double threshold based spectrum sensing for cognitive radio networks,” *International Journal of Energy, Information and Communications*, vol. 5, no. 6, pp. 1–16, 2014.
 - [27] A. Richardson, “Nonparametric statistics for non-statisticians: A step-by-step approach by gregory w. corder, dale i. foreman,” *International Statistical Review*, vol. 78, no. 3, pp. 451–452, 2010.
 - [28] X. Liu, M. Jia, X. Zhang, and W. Lu, “A novel multichannel internet of things based on dynamic spectrum sharing in 5g communication,” *IEEE Internet of Things Journal*, vol. 6, no. 4, pp. 5962–5970, 2018.
 - [29] X. Liu and X. Zhang, “Noma-based resource allocation for cluster-based cognitive industrial internet of things,” *IEEE Transactions on Industrial Informatics*, 2019.
 - [30] M. Dohler and Y. Li, *Cooperative communications: hardware, channel and PHY*. John Wiley & Sons, 2010.
 - [31] R. Gustafsson and A. Mohammed, “Simulation of wireless fading channels,” tech. rep., 2003.
 - [32] B. Luo, P. L. Yeoh, R. Schober, and B. S. Krongold, “Optimal energy beamforming for distributed wireless power transfer over frequency-selective channels,” in *ICC 2019-2019 IEEE International Conference on Communications (ICC)*, pp. 1–6, IEEE, 2019.
 - [33] S. Miller and D. Childers, *Probability and random processes: With applications to signal processing and communications*. Academic Press, 2012.
 - [34] D. P. Doane, “Aesthetic frequency classifications,” *The American Statistician*, vol. 30, no. 4, pp. 181–183, 1976.
 - [35] N. Otsu, “A threshold selection method from gray-level histograms,” *IEEE Transactions on Systems, Man, and Cybernetics*, vol. 9, pp. 62–66, jan 1979.
 - [36] H. Eiselt and C.-L. Sandblom, “Heuristic algorithms,” in *Integer Programming and Network Models*, pp. 229–258, Springer, 2000.
 - [37] D. M. Dobkin, *The RF in RFID: UHF RFID in practice*. Newnes, 2012.
 - [38] V. H. Thanh, R. Zunino, and C. Priami, “Efficient constant-time complexity algorithm for stochastic simulation of large reaction networks,” *IEEE/ACM Transactions on Computational Biology and Bioinformatics (TCBB)*, vol. 14, no. 3, pp. 657–667, 2017.
 - [39] B. Chandramouli and J. Goldstein, “Patience is a virtue: Revisiting merge and sort on modern processors,” in *Proceedings of the 2014 ACM*

SIGMOD international conference on Management of data, pp. 731–742, ACM, 2014.

- [40] T. Fawcett, “An introduction to ROC analysis,” *Pattern recognition letters*, vol. 27, no. 8, pp. 861–874, 2006.
- [41] A. J. Onumanyi, A. M. Abu-Mahfouz, and G. P. Hancke, “A comparative analysis of local and global adaptive threshold estimation techniques for energy detection in cognitive radio,” *Physical Communication*, vol. 29, pp. 1–11, Apr. 2018.
- [42] IEEE802.22, “Enabling broadband wireless access using cognitive radio technology and spectrum sharing in white spaces,” techreport, IEEE, pp. 1 - 20, 2011.
- [43] A. J. Onumanyi, “Dataset for testing the performance of the nonparametric amplitude quantization method,” *Mendeley Data*, v1, Aug. 2018.